Supplementary Information

Tunable band alignment and large power conversion efficiency in two dimensional $InS/ZnIn_2S_4$ van der Waals heterostructure

Hui-Ying Liu[1], Heng-Fu Lin[1,2†], Lu-Ya Xu[1], Ting-Ping Hou[1,2], and Nan-Shu Liu[3†]

[1]Hubei Province Key Laboratory of Systems Science in Metallurgical Process, and College of Science, Wuhan University of Science and Technology, Wuhan 430081, China

[2]The State Key Laboratory for Refractory Material and Metallurgy, International Research Institute for Steel Technology, and Collaborative Center on Advanced Steels, Wuhan University of Science and Technology, Wuhan 430081, China

[3] Chongqing Key Laboratory of Micro & Nano Structure Optoelectronics, School of Physical Science and Technology, Southwest University, Chongqing 400715, China

[†] Corresponding author. Email: hflin@wust.edu.cn (H. F. Lin), liuns0215@gmail.com (N. S. Liu),.

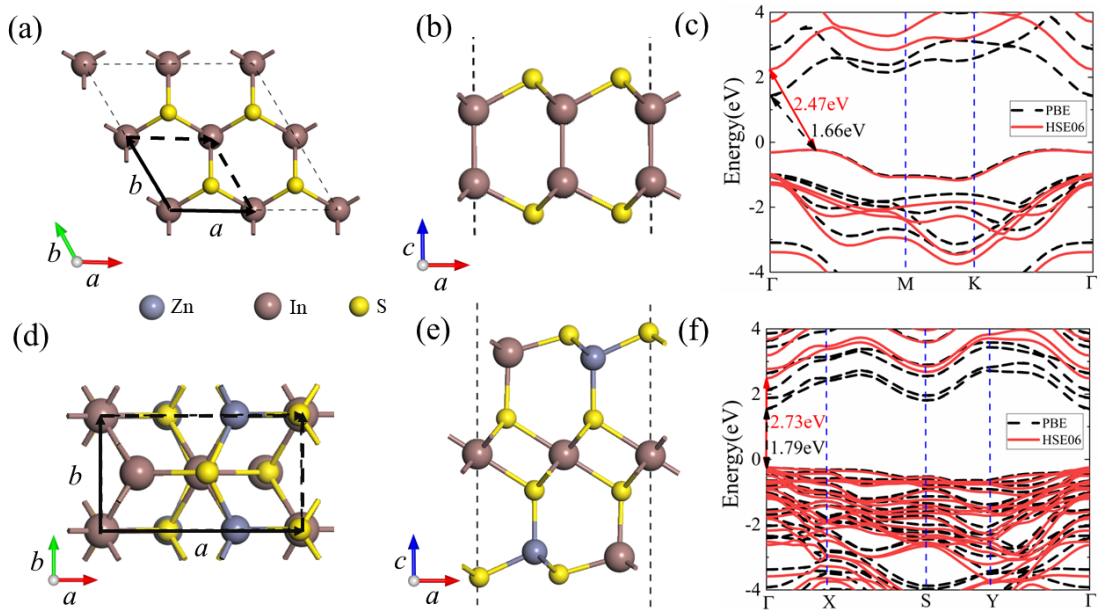

Fig. S1. Top and side views of InS monolayer [(a) and (b)] and $ZnIn_2S_4$ monolayer [(d) and (e)]. The black line in (a) and (d) indicates the unit cell. The band structures of InS monolayer (c) and $ZnIn_2S_4$ monolayer (f).

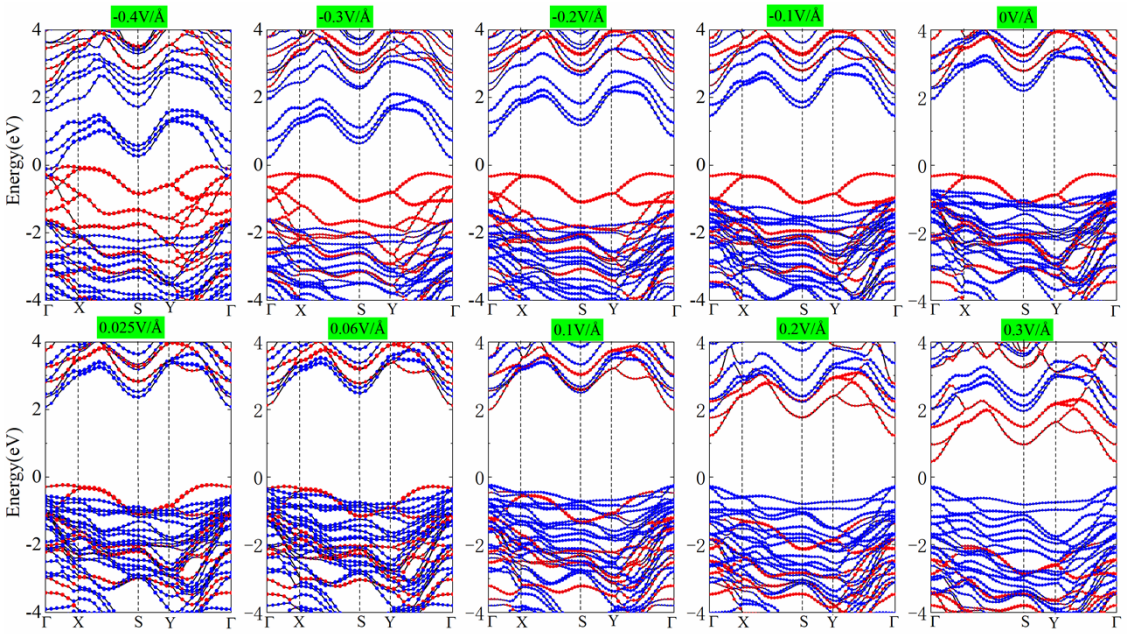

Fig. S2. The projected band structures of the $InS/ZnIn_2S_4$ heterostructure under electric field ranging from −0.4 to 0.3 V/Å.

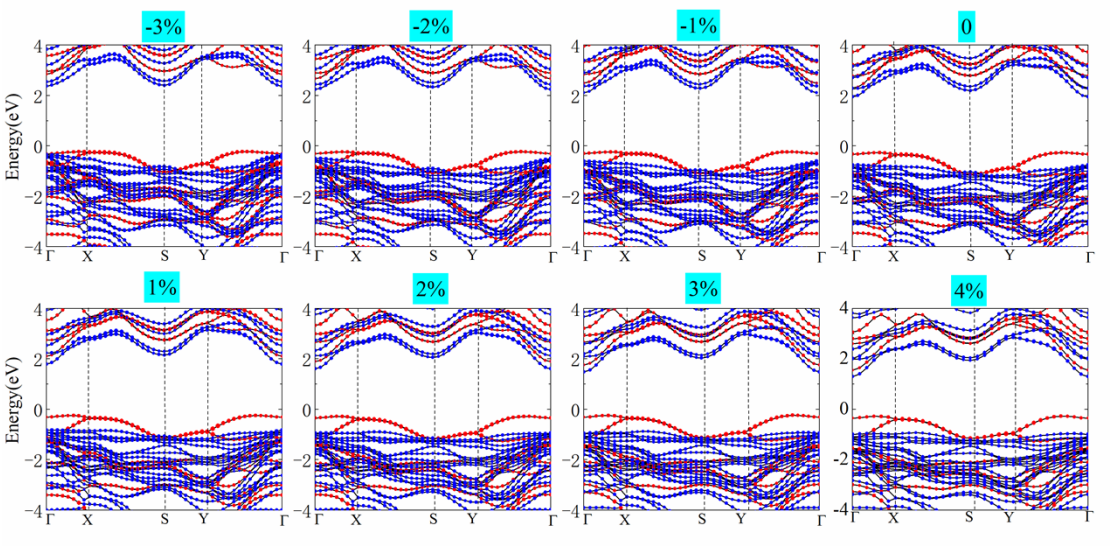

Fig. S3. The projected band structures of $InS/ZnIn_2S_4$ heterostructure with different biaxial strains. The Fermi levels are set to zero.

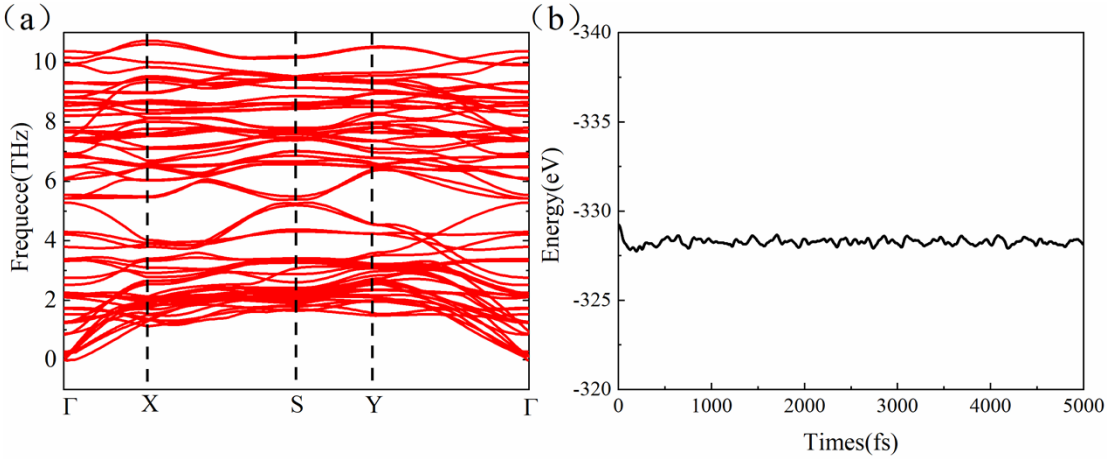

Fig. S4. Phonon spectrums of InS/$ZnIn_2S_4$ heterostructure (a), the variation of total energy of Ga_2SeTe/In_2SSe (HS1-AB) vdw heterostructures as a function of time at temperature 300 K(b).

Table S1. The calculated lattice constants (a and b), equilibrium interlayer distance (d), and binding energy (E_b) of the InS/$ZnIn_2S_4$ heterostructures with different stacking configuration.

	***a*(Å)**	***b*(Å)**	***d*(Å)**	***E*$_b$(meV)**
AA	6.796	3.929	3.71	-25.1
AB	6.796	3.928	3.77	-14.9
AC	6.795	3.926	4.19	-9.6
AD	6.795	3.928	4.03	-11.7

Table S2. The calculated η of the InS/$ZnIn_2S_4$ heterostructure under different electric field $E_{\perp}$. The relevant parameters for the η, E_g^d, Jsc/Psolar, ΔE_c, and V_{oc}, are also provided.

$E_{\perp}$	E_g^d [eV]	Jsc/Psolar	ΔEc [eV]	Voc [V]	η(%)
-0.3	2.63	0.078	2.17	0.16	0.81
-0.2	3.02	0.032	1.91	0.81	1.68
-0.1	2.61	0.081	0.90	1.41	7.42
0	2.57	0.087	0.36	1.91	10.80
0.025	2.59	0.085	0.28	2.01	11.10
0.1	2.60	0.082	0.37	1.93	10.29
0.2	2.24	0.155	0.73	1.21	12.19
0.3	1.84	0.245	1.09	0.45	7.17

Table S3. The calculated η of the $InS/ZnIn_2S_4$ heterostructure under different biaxial strains ε. The relevant parameters for the η, E_g^d, *J*sc/*P*solar, ΔE_c, and V_{oc}, are also provided.

ε(%)	E_g^d [eV]	***J*sc/*P*solar**	**Δ*E*c [eV]**	***V*oc [V]**	**η(%)**
-3	3.07	0.028	0.47	2.30	4.18
-2	2.90	0.042	0.43	2.17	5.92
-1	2.73	0.065	0.38	2.05	8.66
0	2.57	0.087	0.36	1.91	10.80
1	2.35	0.127	0.32	1.73	14.28
2	2.18	0.163	0.30	1.58	16.74
3	2.00	0.205	0.28	1.42	18.92
4	1.83	0.252	0.26	1.27	20.80

Table S4. Calculated carrier effective mass ($m*$), deformation potential constant (E_l), and carrier mobility (μ) for electron (e) and hole (h) along the zigzag (x) and armchair (y) directions at 300 K in $InS/ZnIn_2S_4$ heterostructure

Carrier type	$m^*_x(m_0)$	$m^*_y(m_0)$	$E_{lx}(eV)$	$E_{ly}(eV)$	μ_x ($cm^2\ V^{-1}\ s^{-1}$)	μ_y ($cm^2\ V^{-1}\ s^{-1}$)
Electron	1.49	1.28	-8.35	-8.72	2091.06	2231.94
Hole	0.99	1.01	-9.28	-7.00	3481.04	6118.01